ISSN 1054-660X, Laser Physics, 2009, Vol. 19, No. 5, pp. 1072–1078.

Dynamical Properties of a Rotating Bose–Einstein Condensate[1]

S. Kling[a], * and A. Pelster[b, c], **

[a] *Institut für Angewandte Physik, Universität Bonn, Wegelerstraße 8, 53115 Bonn, Germany*
[b] *Institut für Theoretische Physik, Freie Universität Berlin, Arnimallee 14, 14195 Berlin, Germany*
[c] *Fachbereich Physik, Universität Duisburg-Essen, Lotharstraße 1, 47048 Duisburg, Germany*
*e-mail: kling@iap.uni-bonn.de
**e-mail: axel.pelster@fu-berlin.de
Received 9 March, 2009

Abstract—Within a variational approach to solving the Gross-Pitaevskii equation we investigate dynamical properties of a rotating Bose–Einstein condensate confined in an anharmonic trap. In particular, we calculate the eigenfrequencies of low-energy excitations out of the equilibrium state and the aspect ratio of the condensate widths during the free expansion.

PACS numbers: 03.75.Kk

DOI: 10.1134/S1054660X0905034X

1. INTRODUCTION

The rotation of a Bose–Einstein condensate (BEC) has raised enormous interest, both experimentally and theoretically over the last few years [1]. The BEC is a super-fluid, hence its rotational behavior is quite different from that of a normal fluid. Its properties strongly depend on the specific trap in which it is confined. In harmonic rotating traps centrifugal forces may break the confinement as the rotation frequency approaches the trapping frequency. To overcome this centrifugal barrier, one must increase the strength of the radial confinement. The most natural approach is to add a radial quartic potential to the harmonic trap. Such an anharmonic trap was realized in a recent experiment in Paris at the École Normale Supérieure (ENS) in the group of J. Dalibard in which the centrifugal limit can be exceeded slightly [2, 3]. This combined trap changes both the thermodynamical and the dynamical properties of the condensate drastically, in particular in the fast rotation regime. Nevertheless, the experimental data has been for the most part analyzed considering only the harmonic trapping. This approximation is valid for slow rotation frequencies, but a correct interpretation of the experimental data in the fast rotation regime necessitates an analysis for the full anharmonic trap. Whereas the preceding paper [4] elaborates within the semiclassical approximation the thermodynamical properties of such a rotating BEC, including for instance the critical temperature and the heat capacity, the present work investigates the corresponding dynamical properties. To this end, we proceed as follows. Section 2 introduces the basic Gross–Pitaevskii equation for the condensate wave function of a rotating trapped BEC. Neglecting the emergence of vortices, we determine in Section 3 the stationary equilibrium density of a rotating condensate within the Thomas–Fermi approximation. In Section 4 we then use a variational approach to investigate the hydrodynamic modes of the condensate and its free expansion after switching off the trap. All results are obtained for the specific parameters of the Paris experiment [2, 3].

2. HYDRODYNAMIC FORMALISM

At zero temperature, the dynamics of a BEC is described by the Gross–Pitaevskii Lagrangian density [5, 6]

$$\mathscr{L} = i\hbar\psi^*\frac{\partial}{\partial t}\psi - \frac{\hbar^2}{2M}\nabla\psi^*\cdot\nabla\psi - V(\mathbf{x})\psi^*\psi - \frac{2\pi\hbar^2 a_s}{M}(\psi^*\psi)^2. \tag{1}$$

Here, $V(\mathbf{x})$ denotes the trapping potential, a_s the s-wave scattering length, and M the atomic mass. The transformation into the rotating frame has the consequence that an angular momentum $-\boldsymbol{\Omega}\hat{\mathbf{L}}$ is added to the Lagrangian (1), where the rotation vector is denoted by $\boldsymbol{\Omega} = \Omega\mathbf{e}_z$ and $\hat{\mathbf{L}}$ represents the one-particle quantum mechanical angular momentum operator [7, 8]. The Euler–Lagrange equation then yields the Gross-Pitaevskii (GP) equation

$$i\hbar\frac{\partial}{\partial t}\psi = \left[-\frac{\hbar^2}{2M}\Delta + V(\mathbf{x}) + \frac{4\pi\hbar^2 a_s}{M}|\psi|^2 + \boldsymbol{\Omega}\hat{\mathbf{L}}\right]\psi, \tag{2}$$

Performing the decomposition $\psi = |\psi|e^{iS}$ we work out the hydrodynamic aspects of the system, with condensate density $n = |\psi|^2$ and superfluid velocity $\mathbf{v}_s = \hbar\nabla S/M$.

[1] The article is published in the original.

Basic manipulations yield the coupled hydrodynamic equations, consisting of a continuity equation

$$\frac{\partial}{\partial t}n = -\nabla[(\mathbf{v}_s - \mathbf{v}_{sb})n] \quad (3)$$

and the Euler equation

$$M\frac{\partial}{\partial t}\mathbf{v}_s = -\nabla\left[\frac{M}{2}(\mathbf{v}_s - \mathbf{v}_{sb})^2 - \frac{\hbar^2}{2M}\frac{\Delta\sqrt{n}}{\sqrt{n}} + V(\mathbf{x}, \Omega) + \frac{4\pi\hbar^2 a_s}{M}n\right]. \quad (4)$$

Here $V(\mathbf{x}, \Omega) = V(\mathbf{x}) - M\Omega^2(x^2 + y^2)/2$ stands for the effective potential in the rotating frame and the solid-body velocity is denoted by $\mathbf{v}_{sb} = \mathbf{x} \times \mathbf{\Omega}$. In the following, we consider the cylindrical anharmonic trap used in the Paris experiment [2, 3]

$$V(\mathbf{x}, \Omega) = \frac{M}{2}(\omega_\perp^2 - \Omega^2)r_\perp^2 + \frac{M}{2}\omega_z^2 z^2 + \frac{k}{4}r_\perp^4, \quad (5)$$

where M is the atomic mass of ^{87}Rb, $\omega_\perp = 2\pi \times 64.8$ Hz, $\omega_z = 2\pi \times 11.0$ Hz, $k = 2.6 \times 10^{-11}$ J m^{-4}, and $r_\perp = \sqrt{x^2 + y^2}$. A condensation of 3×10^5 atoms was realized and the highest achieved rotation speed was $\Omega_{max} \approx 1.04\omega_\perp$.

The superfluid is irrotational, i.e. $\nabla \times \mathbf{v}_s = 0$, except at singularities. Since $\nabla \times \mathbf{v}_{sb} = -2\mathbf{\Omega}$, the difference $\mathbf{v}_s - \mathbf{v}_{sb}$ cannot vanish identically. However, the superfluid can mimic solid-body rotation by forming a uniform array of rectilinear vortices parallel to the axis of rotation [9], which minimizes the difference $\mathbf{v}_s - \mathbf{v}_{sb}$. In the detailed analysis of [10] it has been shown that the triangular lattice is energetically the most favorable. For a dense vortex lattice it is even justified to neglect in the Euler Eq. (4) the term proportional to the difference $\mathbf{v}_s - \mathbf{v}_{sb}$ [11]. In the following we assume that this approximation is valid and focus on investigating the effect of the centrifugal term in the potential (5).

3. STATIC PROPERTIES

We start by analyzing the static properties of such a condensate following [12]. To this end we separate the time-dependence according to $n = n(\mathbf{x})$ and $S = -\mu t/\hbar + s(\mathbf{x})$, where μ denotes the chemical potential. With this we obtain from the Euler Eq. (4) the stationary hydrodynamic equation

$$\mu = -\frac{\hbar^2}{2Mn}\frac{\Delta\sqrt{n}}{\sqrt{n}} + V(\mathbf{x}, \Omega) + \frac{4\pi\hbar^2 a_s}{M}n. \quad (6)$$

Furthermore, we make the Thomas–Fermi (TF) approximation [13], neglecting the kinetic energy in (6), so that the condensate density reads

$$n^{TF} \approx \frac{M}{4\pi\hbar^2 a_s}[\mu - V(\mathbf{x}, \Omega)]\Theta[\mu - V(\mathbf{x}, \Omega)], \quad (7)$$

where the Heaviside function Θ ensures its positivity. The chemical potential is determined by the normalization condition $N = \int d^3x n^{TF}$. The Thomas–Fermi radii for the cylindrically symmetric trap potential (5) read

$$R_z^{TF} = \sqrt{\frac{2\mu}{M\omega_z^2}}, \quad (8)$$

$$R_\perp^{TF} = \sqrt{\frac{M(\Omega^2 - \omega_\perp^2)}{k} + \sqrt{\frac{M^2(\Omega^2 - \omega_\perp^2)^2}{k^2} + \frac{4\mu}{k}}}. \quad (9)$$

We perform the spatial integration in cylindrical coordinates, yielding

$$N = \frac{2\sqrt{2M}\mu^2}{3a_s\sqrt{k}\hbar^2\omega_z}f\left(\frac{M(\omega_\perp^2 - \Omega^2)}{2\sqrt{k\mu}}\right), \quad (10)$$

where the function

$$f(x) = \frac{3\pi}{16}(1 + x^2)^2\left[1 - \frac{2}{\pi}\arcsin\frac{x}{\sqrt{1 + x^2}}\right] - \frac{5x}{8} - \frac{3x^3}{8} \quad (11)$$

has the asymptotic properties

$$f(x) = \begin{cases} x/5 - x^3/35 & \text{for} \quad x \gg 1 \\ 3\pi(x^2 + 1)^2/16 - x - x^3 & \text{for} \quad |x| \ll 1 \\ 3\pi(x^2 + 1)^2/8 - x/5 & \text{for} \quad x \ll -1. \end{cases} \quad (12)$$

As the rotation frequency Ω varies between 0 and $\Omega_{max} = 1.04\omega_\perp$, the argument $x = M(\omega_\perp^2 - \Omega^2)/(2\sqrt{k\mu})$ of the function (11) ranges between $-\infty < x < 3.3$. A slow rotation corresponds to $x \gg 1$, in which case the chemical potential reads

$$\mu \approx \hbar\omega_z\left[\frac{15a_s N\sqrt{M}(\omega_\perp^2 - \Omega^2)}{4\sqrt{2\hbar\omega_z^3}}\right]^{2/5} \times\left\{1 + \frac{4k[15a_s N\sqrt{M}(\omega_\perp^2 - \Omega^2)]^{5/2}}{35M^2(\omega_\perp^2 - \Omega^2)^2\sqrt{\hbar\omega_z^3}}\right\}. \quad (13)$$

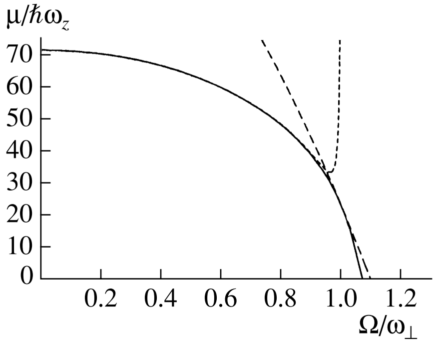

Fig. 1. Chemical potential versus rotation frequency for the parameters of the Paris experiment [2, 3]. The solid line corresponds to (10), the short-dashed and the long-dashed line to the approximations (13) and (14), respectively.

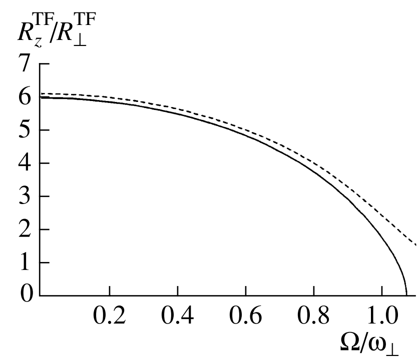

Fig. 2. Aspect ratio of condensate radii versus rotation frequency for the parameters of the Paris experiment [2, 3]. Solid line corresponds to the Thomas–Fermi radii $R_z^{\mathrm{TF}}/R_\perp^{\mathrm{TF}}$, dashed line to the stationary radii $W_{0z}^{\mathrm{TF}}/W_{0x}^{\mathrm{TF}}$ determined from Eq. (21) in Section 4.2.

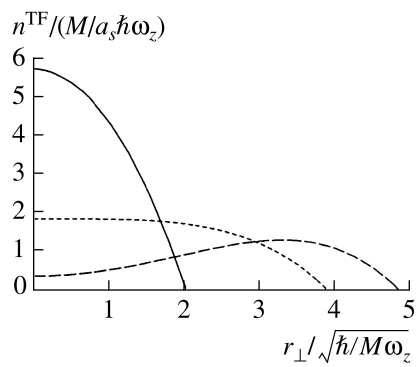

Fig. 3. Thomas–Fermi density (7) in the *xy*-plane for the values of the Paris experiment [2, 3] and various rotation frequencies Ω. From top to bottom the rotation frequencies are $\Omega/\omega_\perp = 0$ (solid), $\Omega/\omega_\perp = 1$ (short-dashed) and $\Omega/\omega_\perp = 1.06$ (long-dashed).

For the fast rotation regime $\Omega \sim \omega_\perp$ we use the expansion (12) for $|x| \ll 1$ and obtain for the chemical potential

$$\mu \approx \hbar\omega_z\left(\frac{32N^2a_s^2k}{\pi^2M\omega_z^2}\right)^{1/4} \times\left[1+\frac{4}{3\pi}\left(\frac{32N^2a_s^2k}{\pi^2M\omega_z^2}\right)^{1/8}\frac{M(\omega_\perp^2-\Omega^2)}{\sqrt{\hbar\omega_z k}}\right]. \tag{14}$$

For an arbitrary rotation frequency Ω the chemical potential follows directly from numerically inverting (10). In Fig. 1 we observe that the chemical potential vanishes for the experimental parameters of the Paris experiment [2, 3] at a critical rotation frequency $\Omega_c \approx 1.07\omega_\perp$. Our assumption, that this indicates the emergence of an instability, is confirmed by evaluating the TF radii (8), (9) and the TF density (7). Figure 2 shows that the TF radius in the *z*-direction vanishes with the chemical potential, being proportional to its square root, while the radius in the perpendicular plane remains finite. Note that the vanishing of one TF radius signals the breakdown of the validity of the TF approximation. Thus, our TF value $\Omega_c \approx 1.07\omega_\perp$ for the critical rotation frequency should be modified by a full quantum mechanical calculation. In Fig. 3 the TF density is shown for three particular rotation frequencies. For an overcritical rotation $\Omega > \omega_\perp$, we notice a pronounced dell in the density profile. Thus, we can conclude from Figs. 1–3 that our TF analysis for the stationary condensate density qualitatively agrees with the experimental finding that the rotation frequency can only be increased until $\Omega_{\max} \approx 1.04\omega_\perp$ [2, 3].

4. DYNAMIC PROPERTIES

In order to investigate the dynamical properties of the condensate, we return to the Euler Eq. (4) in the TF approximation and consider collective excitations of the stationary state. Thus, we look for solutions of the type $n(\mathbf{x}, t) = n^{\mathrm{TF}}(\mathbf{x}) + \delta n(\mathbf{x})e^{i\omega t}$, where $n^{\mathrm{TF}}(\mathbf{x})$ is the stationary TF density (7) and $\delta n(\mathbf{x})e^{i\omega t}$ a small time-dependent deviation. Analogously, the superfluid velocity field is decomposed according to $\mathbf{v}_s = \mathbf{v}_{sb} + \delta\mathbf{v}$. In first order of δn and $\delta\mathbf{v}$ we obtain the eigenmode equation by taking the time derivative of the Euler equation (4) and inserting the continuity Eq. (3)

$$M\omega^2\delta n = -[\mu - V(\mathbf{x}, \Omega)]\nabla^2\delta n + \nabla V(\mathbf{x}, \Omega)\cdot\nabla\delta n, \tag{15}$$

where the chemical potential is a constant which is determined from normalizing the stationary density as described in the previous section. The eigenmode Eq. (15) has been solved analytically for a harmonic trap which is isotropic [14] or rotationally symmetric [15]. However, investigating Eq. (15) for the anharmonic trap, we observe that the differential operator does not conserve powers of the radial coordinate $r_\perp$, so that we may not expect simple analytical solutions. In the special case of an overcritical rotation $\Omega > \omega_\perp$ an analytical solution of (14) has been found in [17].

Another way to obtain the eigenmodes at least approximately is to use a variational approach based on Ritz's method. This method has already been successfully applied for a harmonic trap [16] and is in agreement with the solution of (15) for a large two-particle δ-interaction, i.e. the regime where the TF approximation is valid. For a simplified one- and two-dimensional case this method has already been applied for the anharmonic trap (5) [18, 19]. However, a correct description involves a full three-dimensional treatment which we present now.

4.1. Variational Method

For our variational approach we follow [16] and use a Gaussian shaped condensate

$$\psi(\mathbf{x}, t) = \frac{1}{\sqrt{\pi^{3/2} W_x W_y W_z}} \exp\left\{-\frac{x^2}{2W_x^2} - \frac{y^2}{2W_y^2} - \frac{z^2}{2W_z^2} + i[S_x x^2 + S_y y^2 + S_z z^2]\right\}, \tag{16}$$

where $W_{x,y,z}$ and $S_{x,y,z}$ denote time-dependent variational parameters for the widths and the phases, respectively. Note that (16) can only be used in the undercritical regime $\Omega \le \omega_\perp$. For $\Omega > \omega_\perp$ a central hole emerges in the condensate (see Fig. 3), which is not described by the Gaussian trial function. For the ansatz (16) we determine the Lagrangian $L = \int d^3x \mathcal{L}$ with the density (1) and the potential (5). Thus, the resulting action $A = \int dt L$ represents a functional of the trial functions $W_{x,y,z}$ and $S_{x,y,z}$ which are determined according to the Hamilton principle. As we find for the phases the relation $S_{x,y,z} = -\dot{W}_{x,y,z}/2W_{x,y,z}$ we can eliminate them and find for the widths the coupled equations of motion

$$\frac{d^2}{dt^2}W_{x,y} = -\lambda^2\eta W_{x,y} + \frac{1}{W_{x,y}^3} + \frac{P}{W_{x,y}^2 W_{y,x} W_z} - \kappa(3W_{x,y}^3 + W_{x,y}W_{y,x}^2),$$
$$\frac{d^2}{dt^2}W_z = -W_z + \frac{1}{W_z^3} + \frac{P}{W_x W_y W_z^2}, \tag{17}$$

where we have introduced the dimensionless variables $\lambda = \omega_\perp/\omega_z \approx 6$, $\eta = 1 - (\Omega/\omega_\perp)^2$, and $\kappa = k\hbar\omega_z/a_z^4 \approx 0.4$. The length scale is set by the harmonic oscillator length $a_z = \sqrt{\hbar/M\omega_z} \approx 3.2$ μm, so that $W_{x,y,z} \longrightarrow W_{x,y,z}a_z$, and the time is scaled by $t \longrightarrow t/\omega_z$. The resulting dimensionless interaction parameter is denoted by $P = \sqrt{2/\pi} N a_s/a_z \approx 374$, where we have used the s-wave scattering length $a_s = 5$ nm of ^{87}Rb. The term proportional to κ is due to the anharmonicity of the trap and represents the main difference in comparison with the treatment of the harmonic trap in [16]. The Euler–Lagrange Eqs. (17) are of the form $\ddot{W}_{x,y,z} = -\partial V_{\text{eff}}(W_x, W_y, W_z)/\partial W_{x,y,z}$ and can therefore be regarded as the motion of a fictitious point particle in the effective potential

$$V_{\text{eff}}(\mathbf{W}) = \frac{\lambda^2\eta}{2}W_x^2 + \frac{\lambda^2\eta}{2}W_y^2 + \frac{1}{2W_x^2} + \frac{1}{2W_y^2} + \frac{\kappa}{4}(3W_x^4 + 2W_x^2W_y^2 + 3W_y^4) + \frac{1}{2}W_z^2 + \frac{1}{2W_z^2} + \frac{P}{W_xW_yW_z}, \tag{18}$$

where the vector of the widths is denoted by $\mathbf{W} = (W_x, W_y, W_z)$.

4.2. Low-Energy Excitations

At first, we determine the optimal widths of the equilibrium state around which the density fluctuates. The stationary point is obtained by setting $\ddot{W}_{0k} = 0$, yielding a set of algebraic equations. Because of the rotational symmetry of the trap we have $W_{0x} = W_{0y}$, thus the stationary widths follow from

$$\lambda^2\eta W_{0x} = \frac{1}{W_{0x}^3} + \frac{P}{W_{0x}^3 W_{0z}} - 4\kappa W_{0x}^3,$$
$$W_{0z} = \frac{1}{W_{0z}^3} + \frac{P}{W_{0x}^2 W_{0z}^2}. \tag{19}$$

Considering small deviations from the equilibrium state, we perform a Taylor approximation of the effective potential $V_{\text{eff}}(\mathbf{W}) \approx V_{\text{eff}}(\mathbf{W}_0) + \delta\mathbf{W}H\delta\mathbf{W}^T/2$, where $\mathbf{W}_0$ denotes the stationary point and H is the Hessian matrix. The square-root of the eigenvalues of H are the low excitation frequencies, for which we find the analytical expressions

$$\omega_1 = 2\omega_z\sqrt{\lambda^2\eta + 5\kappa W_{0x}^2 - 2P_{4,1}},$$
$$\omega_{2,3} = \sqrt{2}\omega_z\left(1 + \lambda^2\eta + 6\kappa W_{0x}^2 - P_{2,3} \pm \sqrt{[\lambda^2\eta + 6\kappa W_{0x}^2 - 1 + P_{2,3}]^2 + 8P_{3,2}P_{4,1}}\right)^{1/2}, \tag{20}$$

where we have introduced the notation $P_{i,j} = P/(4W_{0x}^i W_{0z}^j)$. The corresponding TF approximation

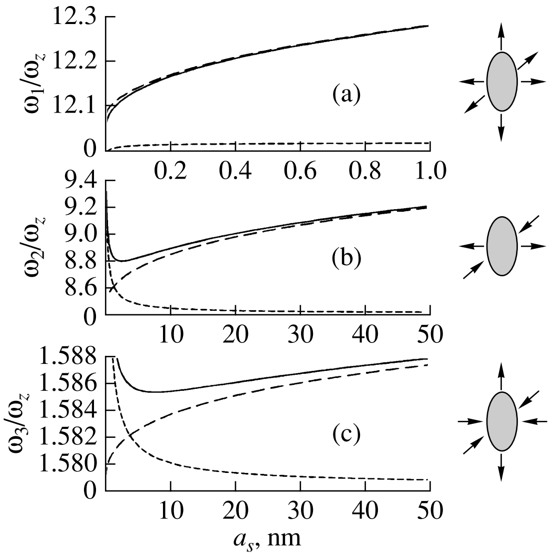

Fig. 4. Three eigenmodes of the non-rotating condensate ($\Omega = 0$) confined in the anharmonic trap (5): (a) breathing mode, (b) and (c) scissor modes. The solid lines correspond to the solution of the variational procedure (20), the long-dashed lines to its TF approximation (22), and the short-dashed lines to the harmonic trap ($\kappa = 0$). The condensate clouds show the temporal behaviour of the respective eigenmodes.

of these modes follows from neglecting the $1/W^3$-terms in (17) which correspond to the kinetic energy and are here related to a large interaction parameter $P \longrightarrow \infty$. In this case the algebraic Eq. (19) for the stationary widths reduces to

$$P = W_{0x}^{\mathrm{TF2}} W_{0z}^{\mathrm{TF3}}, \quad W_{0z}^{\mathrm{TF2}} = W_{0x}^{\mathrm{TF2}}(\lambda^2\eta + 4\kappa W_{0x}^{\mathrm{TF2}}). \quad (21)$$

The resulting ratio $W_{0z}^{\mathrm{TF}}/W_{0x}^{\mathrm{TF}}$ agrees qualitatively with the aspect ratio of TF condensate radii (see Fig. 2). The oscillation frequencies (20) simplify in the TF approximation to

$$\omega_1^{\mathrm{TF}} = \sqrt{2}\omega_z\sqrt{\lambda^2\eta + 6\kappa W_{0x}^{\mathrm{TF2}}},$$
$$\omega_{2,3}^{\mathrm{TF}} = \sqrt{2}\omega_z(3/4 + \lambda^2\eta + 6\kappa W_{0x}^{\mathrm{TF2}} \quad (22)$$
$$\pm\sqrt{[\lambda^2\eta + 6\kappa W_{0x}^{\mathrm{TF2}} - 3/4]^2 + 2\kappa W_{0x}^{\mathrm{TF2}} + \lambda^2\eta/2})^{1/2}.$$

Figure 4 shows that the three eigenfrequencies (20) and their TF approximation (22) for a non-rotating condensate ($\Omega = 0$) increase with the s-wave scattering length a_s. This effect is due to the presence of the trap anharmonicity, as the eigenfrequencies in a harmonic trap ($\kappa = 0$) tend to a constant in the limit $a_s \longrightarrow \infty$. For ^{87}Rb the s-wave scattering length is about $a_s = 5$ nm, so we can conclude from Fig. 4 that the TF approximation is sufficient for the Paris experiment [2, 3]. Therefore, the strong dependence of the eigenmodes on the rotation frequency Ω is depicted in Fig. 5 only for the TF approximated frequencies (22).

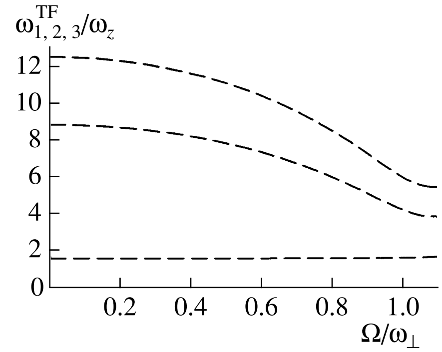

Fig. 5. Eigenfrequencies of the condensate confined in the anharmonic trap (5) in the TF approximation (22).

4.3. Free Expansion

The equations of motion (17) also determine the expansion dynamics of the condensate after switching off the trap. Following [20], we rewrite them within the TF approximation, yielding

$$\ddot{b}_\perp = \frac{\Omega^2 b_\perp}{\omega_z^2} + \frac{\lambda^2\eta + 4\kappa W_{0x}^{\mathrm{TF2}}}{b_\perp^3 b_z}, \quad (23)$$

$$\ddot{b}_z = \frac{1}{b_\perp^2 b_z^2}, \quad (24)$$

where we have introduced the scaling parameters $b_\perp(t) = W_x^{\mathrm{TF}}(t)/W_{0x}^{\mathrm{TF}}$ and $b_z(t) = W_z^{\mathrm{TF}}(t)/W_{0z}^{\mathrm{TF}}$. The initial conditions for the scaling parameters are given by $b_\perp(0) = b_z(0) = 1$ and $\dot{b}_\perp(0) = \dot{b}_z(0) = 0$. The initial velocities vanish at $t = 0$ because of the equilibrium condition. Since we have $\lambda^2\eta + 4\kappa W_{0x}^{\mathrm{TF2}} \gg 1$ for all experimentally realizable rotation frequencies Ω, the expansion in the z-direction is much slower than in the radial direction. Therefore, we may decompose the scaling parameter $b_z = 1 + \epsilon$ and consider ϵ as a small time-dependent quantity. In zeroth order in ϵ we obtain from (23) for the radial scaling parameter

$$b_\perp = \frac{\omega_z}{\sqrt{2}\Omega}[\Omega^2/\omega_z^2 - \lambda^2\eta - 4\kappa W_{0x}^{\mathrm{TF2}}$$
$$+ (\Omega^2/\omega_z^2 + \lambda^2\eta + 4\kappa W_{0x}^{\mathrm{TF2}})\cosh(2\Omega/\omega_z t)]^{1/2}. \quad (25)$$

With this solution we determine the scaling parameter for the expansion in the z-direction by integrating $\ddot{\epsilon} = 1/b_\perp^2$ either numerically or analytically in the limit of

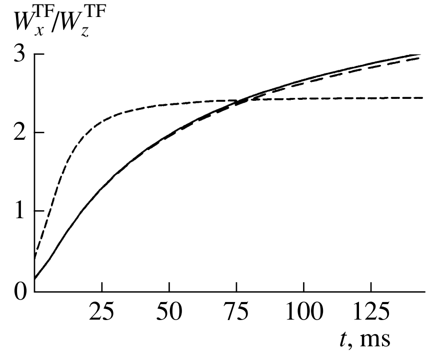

Fig. 6. Aspect ratio of the non-rotating condensate ($\Omega = 0$) for the parameters of the Paris experiment [2, 3]. The solid line corresponds to $\kappa = 0.4$, the long-dashed lines to $\kappa = 0$, and the short-dashed lines to the interaction free Bose gas ($a_s = 0$) with $\kappa = 0.4$.

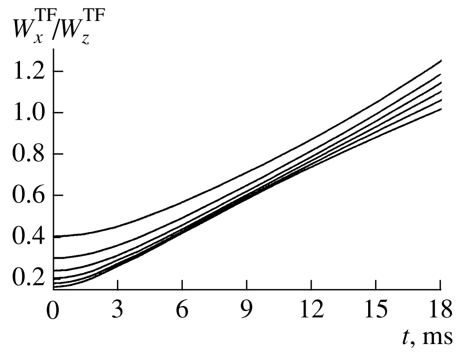

Fig. 7. Aspect ratio of the rotating condensate confined in the Paris trap [2, 3] for various rotation frequencies. The rotation parameter $\eta = 1 - (\Omega/\omega_\perp)^2$ is varied in steps of width 0.2 from 0 (lowest line) to 1 (highest line).

slow and fast rotation frequencies. With this we approximately obtain for $\Omega \ll \omega_z$

$$b_z \approx 1 + \frac{t\arctan\left(\sqrt{\lambda^2\eta + 4\kappa W_{0x}^{TF2}}\,t\right)}{\sqrt{\lambda^2\eta + 4\kappa W_{0x}^{TF2}}} - \frac{\ln[1 + (\lambda^2\eta + 4\kappa W_{0x}^{TF2})t^2]}{2\lambda^2\eta + 8\kappa W_{0x}^{TF2}} + \frac{\Omega t/\omega_z}{\lambda^2\eta + 4\kappa W_{0x}^{TF2}} \qquad (26)$$

and, correspondingly, for $\Omega \approx \omega_z$

$$b_z \approx 1 + \ln\left(\cosh\frac{\Omega t}{\omega_z}\right). \qquad (27)$$

Note the time of flight of the Paris experiment [2, 3] lasts 18 ms. Figure 6 shows that the anharmonicity κ has only a marginal effect on the aspect ratio of the widths $W_x^{TF}/W_z^{TF} = b_x W_{0x}^{TF}/b_z W_{0z}^{TF}$ for a non-rotating condensate ($\Omega = 0$). However, this changes drastically once the condensate is rotating. From Fig. 7 we see that the effect of the trap anharmonicity upon the aspect ratio is significantly enhanced in the fast rotating regime. Therefore, this effect must be taken into account for any analysis of free expansion data for large rotation speeds.

5. CONCLUSIONS

In this paper we have analyzed dynamical properties of a rotating BEC for the specific parameters of the Paris experiment [2, 3]. In doing so we have provided useful theoretical results for future BEC experiments in such anharmonic traps.

At first, we have determined how the stationary TF density profile of the condensate varies with increasing rotation frequency Ω. In the overcritical rotation regime we have found that the density in the center is reduced. Thus, the rotation frequency has a theoretical upper bound of $\Omega_c \approx 1.07\omega_\perp$, which qualitatively agrees with the highest experimentally realized rotation speed of $\Omega_{max} \approx 1.04\omega_\perp$ [2, 3]. This quantitative agreement is astonishing, as we have neglected the presence of vortices in our TF analysis.

Furthermore, we have used a variational approach to find the frequencies of the low-energy excitations which depend strongly on the rotation frequency Ω. The anharmonicity influences the eigenmodes in a characteristic way as it enters the equilibrium state of the condensate. Finally, we have determined the time dependence of the aspect ratio of the condensate widths for the expansion out of the trap which is an important quantity for analyzing the experimental data. The rotation increases significantly the velocity of the expansion in the *xy*-plane. This effect could be used to determine the rotation speed in the experiment.

ACKNOWLEDGMENTS

We thank Kiel Howe for critically reading the manuscript and we acknowledge support from the Priority Program SPP 1116 *Interaction in Ultracold Gases of Atoms and Molecules* of the German Research Foundation (DFG).

REFERENCES

1. I. Bloch, J. Dalibard, and W. Zwerger, Rev. Mod. Phys. **80**, 885 (2008).
2. V. Bretin, S. Stock, Y. Seurin, and J. Dalibard, Phys. Rev. Lett. **92**, 050403 (2004).
3. S. Stock, *Quantized Vortices in a Bose–Einstein Condensate: Thermal Activation and Dynamic Nucleation*, PhD Thesis, Université Paris (2006).
4. S. Kling and A. Pelster, Phys. Rev., Ser. A **76**, 023609 (2007).
5. E. P. Gross, Nuovo Cimento **20**, 454 (1961).
6. L. P. Pitaevskii, JETP **13**, 451 (1961).

7. C. J. Pethick and H. Smith, *Bose–Einstein Condensation in Dilute Gases*, 2nd ed. (Cambridge Univ. Press, Cambridge, 2008).
8. L. P. Pitaevskii and S. Stringari, *Bose–Einstein Condensation* (Science Pub., Oxford, 2003).
9. R. P. Feynman, Prog. Low Temp. Phys. **1**, 17 (1955).
10. V. K. Tkachenko, Sov. Phys. JETP **22**, 1282 (1966).
11. A. L. Fetter, J. A. Sauls, and D. L. Stein, Phys. Rev., Ser. B **28**, 5061 (1983).
12. A. L. Fetter, Phys. Rev., Ser. A **64**, 063608 (2001).
13. G. Baym and C. J. Pethick, Phys. Rev. Lett. **76**, 6 (1996).
14. S. Stringari, Phys. Rev. Lett. **77**, 2360 (1996).
15. M. Fliesser, A. Csordás, P. Szépfalusy, and R. Graham, Phys. Rev., Ser. A **56**, R2533 (1997).
16. V. M. Pérez-Garciá, H. Michinel, J. I. Cirac, M. Lewenstein, and P. Zoller, Phys. Rev. Lett. **77**, 5320 (1996).
17. M. Cozzini, A. L. Fetter, B. Jackson, and S. Stringari, Phys. Rev. Lett. **94**, 100402 (2005).
18. G.-Q. Li, L.-B. Pu, J.-K. Xue, X.-Z. Chen, and J. Liu, Phys. Rev., Ser. A **74**, 055601 (2006).
19. T. K. Ghosh, Phys. Rev., Ser. A **69**, 043606 (2004).
20. Y. Castin and R. Dum, Phys. Rev. Lett. **77**, 5315 (1996).